New ESTER/PHOENICS – An Upgraded 3D MHD Modelling Software for Aluminium Reduction Cells

Vinko Potocnik[1] and John Ludwig[2]
1. Consultant, Jonquière, Québec, Canada
2. Development Manager, Concentration Heat and Momentum Limited (CHAM), Wimbledon Village, London, United Kingdom
Corresponding author: vinko.potocnik@videotron.ca

Abstract

ESTER/PHOENICS is the first 3D MHD commercial software package, developed in the 1980s, that included steady state calculations of the metal and bath velocities, metal heaving and transient calculation of MHD waves of the bath-metal interface. ESTER (Electrolytic SmelTER) is a special purpose adaptation of the general-purpose fluid flow and heat transfer code PHOENICS, dedicated to the MHD of the aluminium electrolysis cells. The original ESTER was limited in geometry to metal pad, bath and anodes to the top of carbon. Electrical boundary conditions required vertical current density distribution at the bottom of metal pad. Magnetic field was also given as an input file or an analytical equation in ESTER, and this remains the same now. The new ESTER upgrade extended the geometry from the end of collector bars to the anode beam (Model 1), so that the calculation of the current distribution in the metal pad does not require external input file. This requires a detailed computational grid to represent the geometry of collector bars correctly, but such a detailed grid cannot be used for transient calculations. Therefore, two submodels for the calculation of waves were built: Model 2 from the bottom of the metal pad to the top of the anode beam and Model 3 from the bottom of the metal pad to the top of anodes, allowing a much coarser grid in order to reduce the transient computation time. In these two submodels, at the bottom boundary, the vertical current density distribution is obtained from the detailed model by automatic interpolation between the fine and the coarse grid. The paper describes the new ESTER structure and some test applications.

Keywords: MHD of aluminium electrolysis cells, Computational fluid dynamics (CFD), ESTER/PHOENICS software package, 3D MHD wave calculations.

1. Introduction

ESTER (Electrolytic SmelTER) is a special purpose adaptation for MHD of aluminium electrolysis cells of the general-purpose fluid flow and heat transfer code PHOENICS. It is attached to PHOENICS as an additional user accessible GROUND station. It makes use of the standard PHOENICS pre- and post-processors for data input and graphical display, ESTER VR-Editor. ESTER can be set-up and run easily by anybody, it does not require any programming skills but, of course, it requires understanding of MHD and busbar design principles to effectively use it for cell design.

ESTER was the first 3D MHD commercial software package, developed in the 1980s, that included steady state calculations of the metal and bath velocities, metal heaving and 3D transient calculation of MHD waves of the bath-metal interface [1]. The capability of wave calculations with application to magnetic compensation loop design of potlines has been recently demonstrated again [2].

The main features of ESTER are:

- It is a 3D code, steady state and transient.
- Turbulence models are included (constant viscosity, k-ε, k-ω and other models).
- Its analysis domain has 3 options with specific electrical boundary conditions for each of these:
    - Model 1: Full model from the end of cathode blocks and collector bars to the top of the anode beam busbar;
    - Model 2: From the top of cathode carbon to the top of the anodes below stubs and;
    - Model 3: From the top of cathode carbon blocks to the top of anode beam busbar.

  For Model 2 and Model 3, the electric current density on the top of cathode block can be imported from Model 1.
- Magnetic field has to be calculated by another program. It can be imported as an external data file represented in analytical form at ESTER input. The default analytical expression is available to all users.
- Anode bottom can be flat or shaped to the metal pad heave, keeping the anode-cathode distance constant for steady-state calculations.
- Individual anodes can be active (carrying current) or inactive (after anode change). Anodes can be raised or lowered.
- Flow induced current density is also calculated, $\mathbf{j}_i = \sigma\, \mathbf{v} \times \mathbf{B}$). This is a toggle (off or on) in ESTER, so that its effects can be easily explored.
- Electric current density is calculated within the conductive parts of the cell. In the liquid metal and bath, the current density is combined with the magnetic field to get the electromagnetic (Lorenz) force **j x B.**
- For transient calculations, initial metal-bath interface can be uniformly inclined in the longitudinal direction or specified in a table.
- ESTER uses floating grid, where the grid plane at the bath-metal interface deforms with the metal heave and keeps the interface always sharply defined. This simplifies the tracking of the interface tremendously and eliminates the need for fine grid and remeshing near the interface, which is required in the volume of fluid (VOF) models used in other models. The gain is much reduced computation time for steady-state, and particularly for wave calculations.

The results are:

- Current densities in the whole domain. Of specific interest are current densities in the liquid metal pad and in the bath;
- Velocities in bath and metal;
- Metal bath interface deformation;
- Flow induced current density;
- Currents in anode rods, anode busbars and collector bars;
- Turbulence parameters and viscosity;
- For transient calculations:
    - Waves, on the metal-bath interface;
    - Oscillations of anode rod currents and
    - Oscillations of cell voltage (cell MHD instability).

2. Geometry

2.1 ESTER Domains

Full ESTER domain is shown in 3D in Figure 1 for a typical cell with 24 anodes and 14 cathode blocks and collector bars. It comprises the domain from the end of cathode blocks to the top anode beam busbars. This is the extension of the original ESTER which comprised the Model 2 domain described in Figure 2. Model 3 includes the same bottom part as Model 2 but the top goes up to the top of the anode beam. Model 2 electrical boundary conditions required vertical current density distribution at the bottom of metal pad, which had to be given as an input file. The new ESTER upgrade extended the geometry from the end of collector bars to the anode beam, so that the calculation of the current distribution in the metal pad does not require external input file. The current density at the top of cathode blocks is calculated in the full Model 1 and written out in a format that can easily be transferred to Model 2 and Model 3. Model 3 is also an extension of the original program.

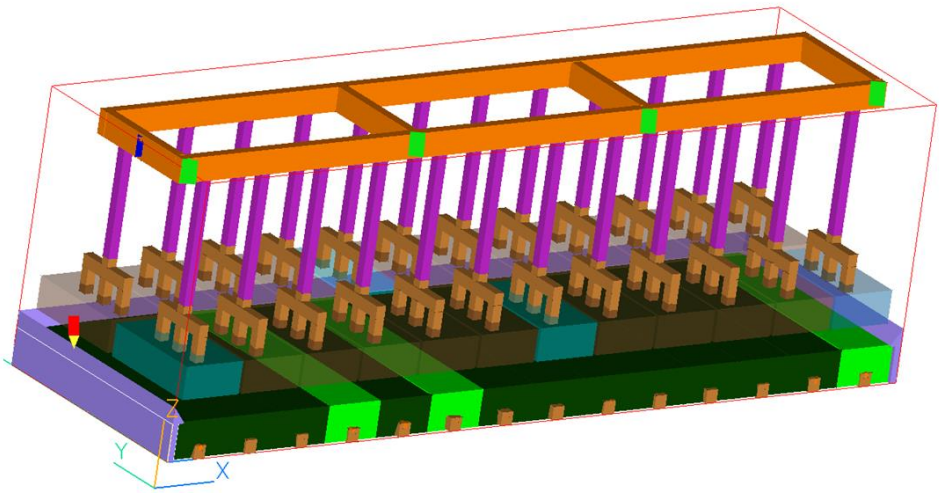

Figure 1. Full ESTER model for a 24-anode cell. Three cathode blocks and 4 anode blocks are shown in brighter colours to enhance the 3D perspective. Green rectangles on the anode beam are current entrance points (the number on the sides and the ends specified by the user). The blue spot at the left end of anode beam is specified reference voltage (from ESTER Library CaseY495).

In the full Model 1, a very fine computational grid is required in the cathode to represent correctly the collector bars, which is no problem for steady-state calculations. With a very fine grid the CPU time is only a few hours, and this is very fast because of floating grid. However, in the wave calculations the CPU time with such a fine grid is still too high for practical design work, and using Model 2 or Model 3 is advantages because a much coarser grid can be used.

The difference between Model 2 and Model 3 is that Model 2 has uniform voltage fixed on top of all the anodes, in other words, an equipotential is fixed there. In fact, a (near) equipotential is on the anode beam which is used in Model 1 and Model 3. The resistance from the top of the anodes to the anode beam damps the current changes in the anodes arising from waves; that means, that Model 2 represents an overestimation of the current driving the waves. However, the overestimation is not very large, because the voltage drops missing on the top in Model 2 are small in comparison to the voltage drop across the anode blocks and the bath below the anodes.

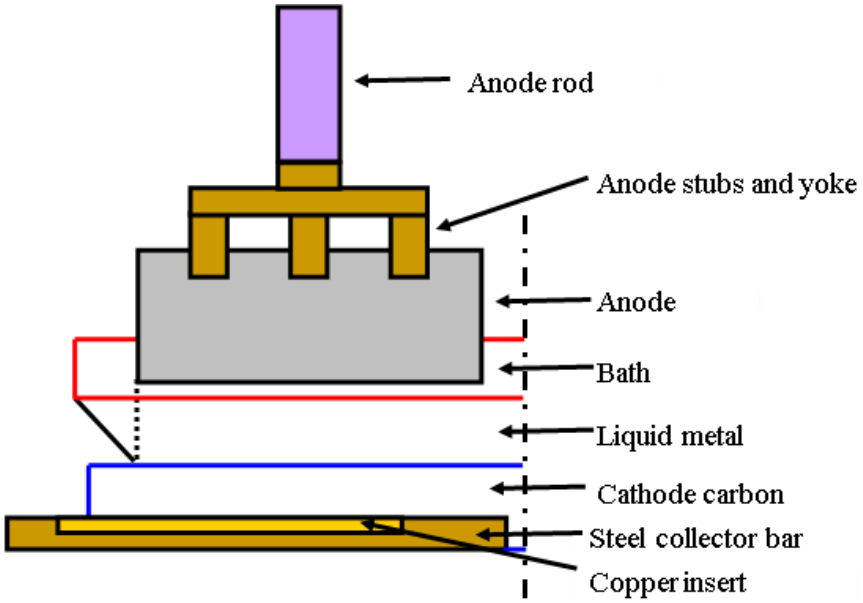

Figure 2. Transverse cross-section of the computational domain for the full model up to the anode beam (Model 1). The simplest (Model 2) domain is from the top of carbon block to the top of the anodes below the stubs. Model 3 is from the top of the cathode block to the top of the anode beam.

It has been shown [1] that a very coarse grid in Model 2 represents very well the MHD wave phenomena in the liquid metal. This brings the wave calculations with ESTER within the reach of practical busbar design studies [2].

2.2 ESTER Geometry Setup Menus

ESTER input preparation is hierarchical menu-driven. The main geometry menu is shown in Figure 3. Figure 4 shows cathode settings and Figure 5 anode settings. Anodes can be active (in normal operation) or not (after anode change), they can be raised or not, according to the specification in anode object attributes.

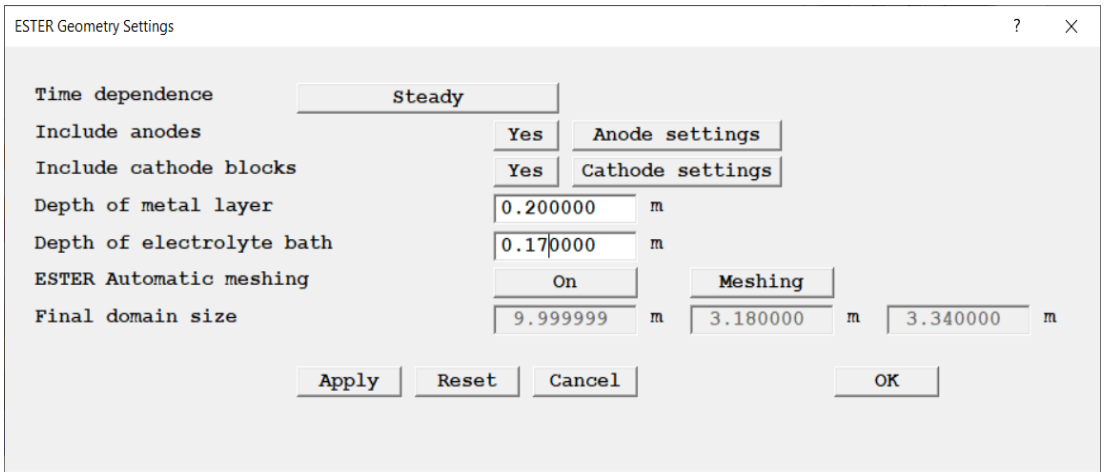

Figure 3. Main geometry settings menu.

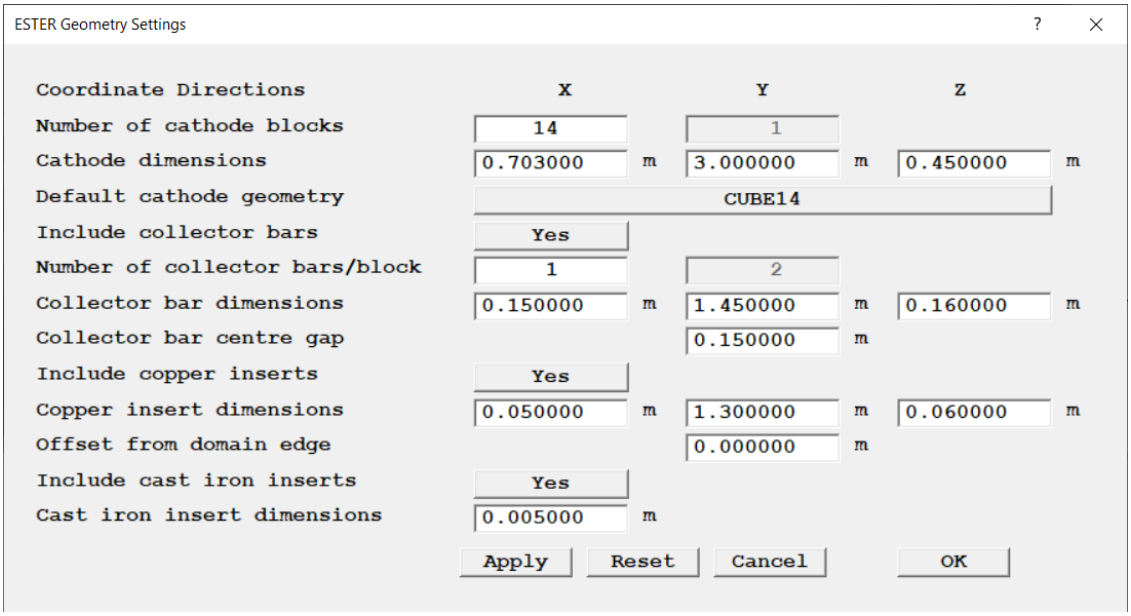

Figure 4. Cathode settings menu.

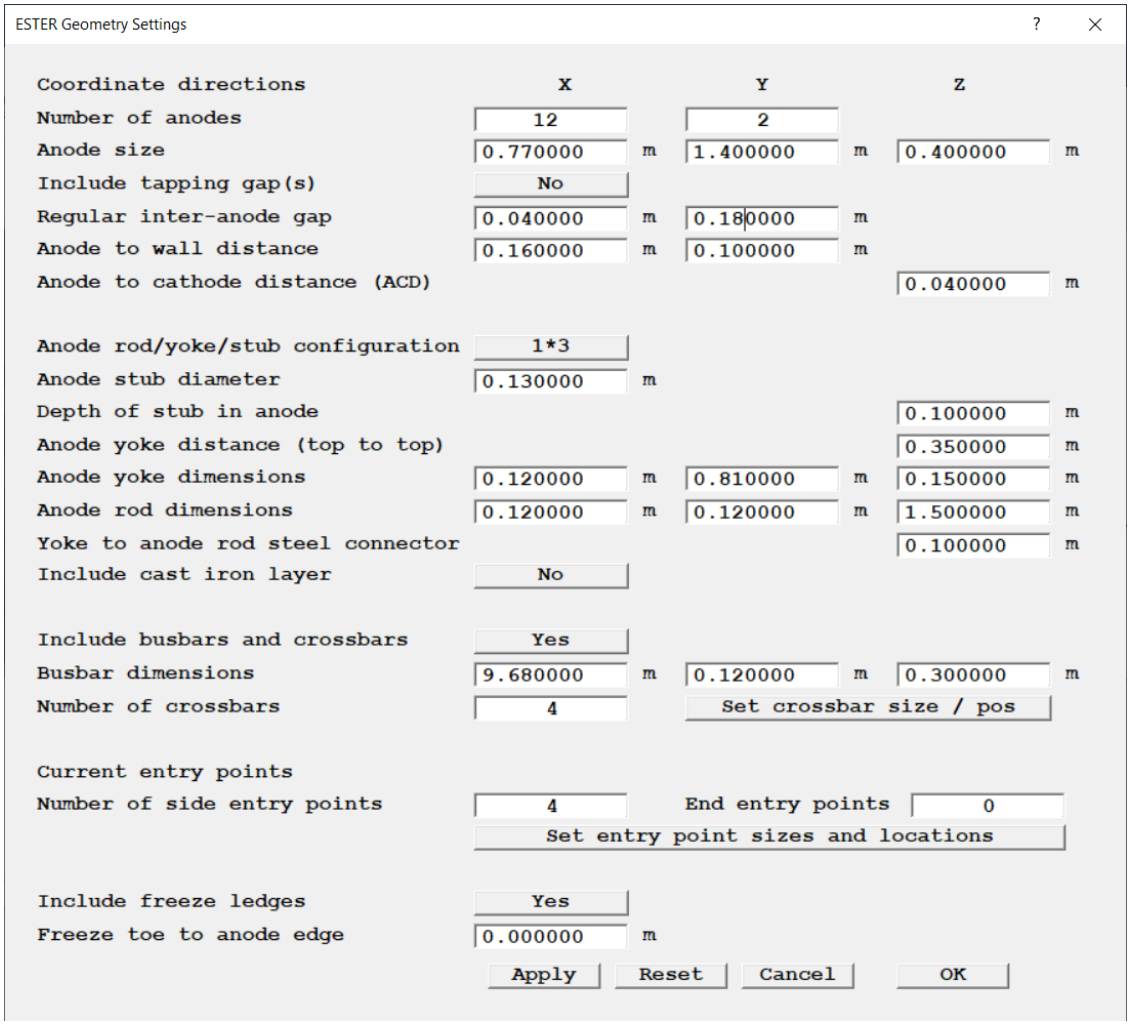

Figure 5. Anode settings menu.

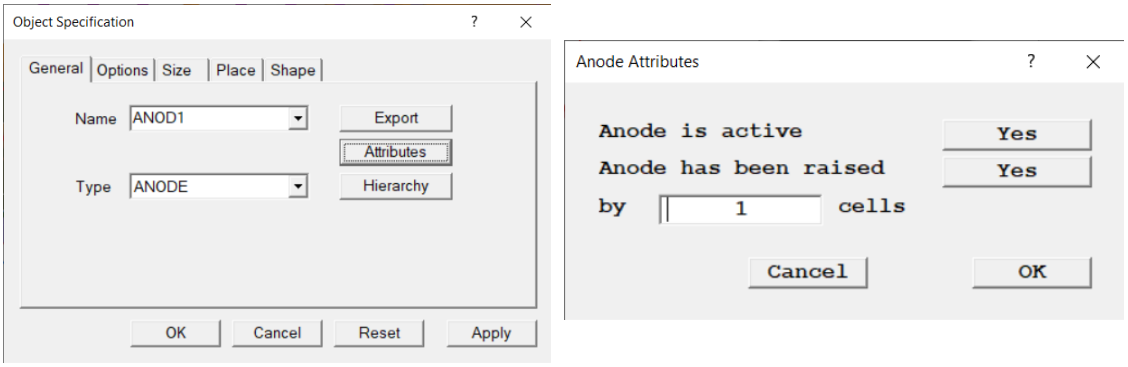

Figure 6. Specification of special state of an anode.

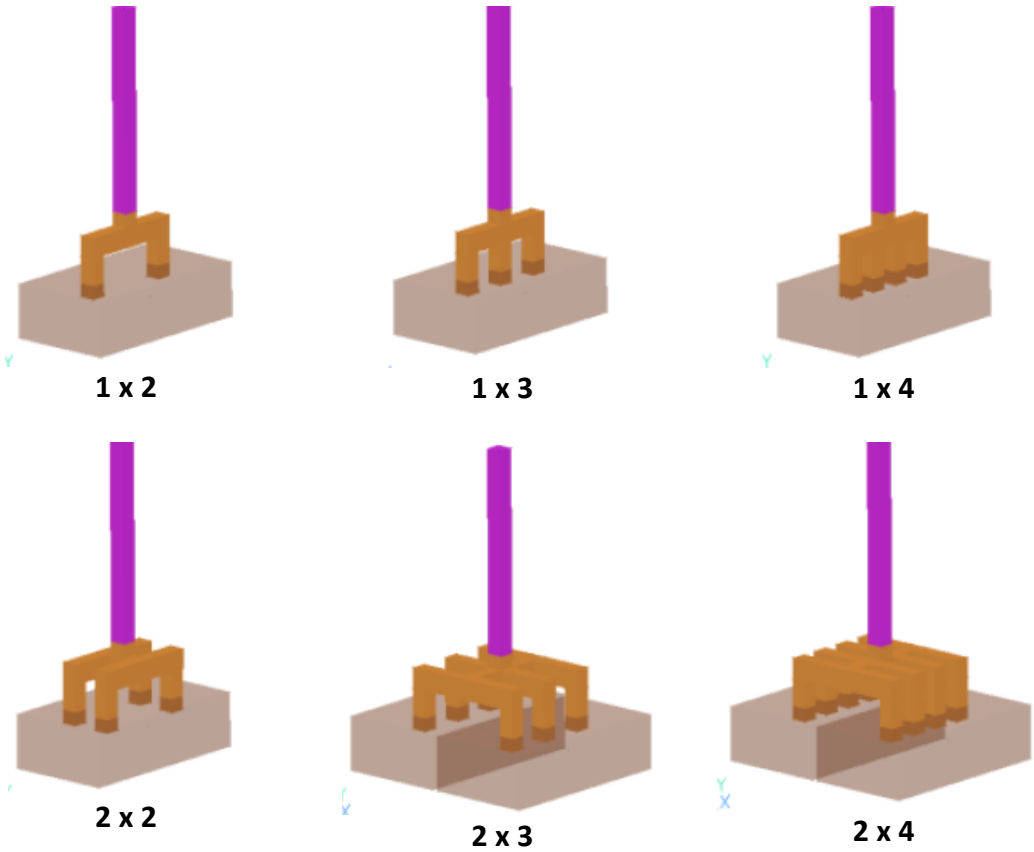

Figure 7. Preprogrammed anode configurations. The m x n nomenclature refers to the number of stubs in x and y direction.

3. Floating Grid

ESTER uses rectangular mesh in x, y and z direction. It is desirable that the grid lines coincide with the edges of objects such as anodes, cathode collector bars, anode rods, etc. An example of the grid is shown in Figure 8. In this case, the anodes are defined with a grid lime at every anode edge; this is important because the channels between anodes must be strictly defined with their true width. On the other hand, the collector bar edges do not fall exactly on the grid. More gridlines would be needed; they could be placed manually to the collector bar edges to give the most accurate and uniform current distribution in the cathode blocks.

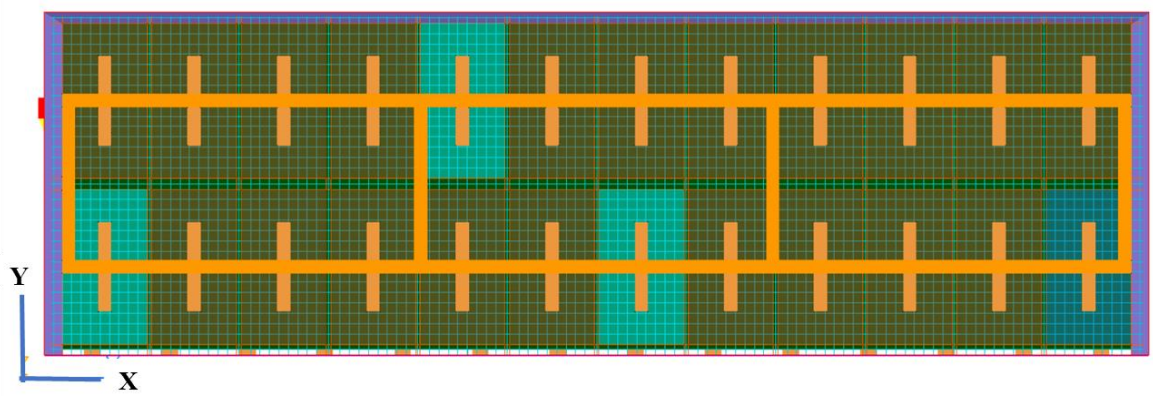

Figure 8. ESTER horizontal mesh and gridlines.

Gridlines in the vertical directions are called slabs. Figure 9 shows the automatic mesh menu with the definition of the slabs.

ESTER Mesh Settings

	X-direction	Y-direction	Z-direction
Cells in anodes	9	15	
Cells in inter-anode	2	2	
Cells in anode to wall	2	2	
Slabs in carbon blocks:			
below copper inserts			2
in copper inserts			2
above copper inserts			4
Slabs in metal			5
Slabs in bath under anodes			4
Slabs in bath at anode immersion			3
Slabs in anodes above bath			3
Slabs in yokes			5
Slabs in rods			10
Slabs in busbars			2
Total number of cells	134	36	40

Apply Reset Cancel OK

Figure 9. Automatic meshing specification menu.

A primary feature of the Hall-Héroult cell is the presence of two distinct layers of immiscible liquids, which never intermingle. The liquid metal is at the bottom, in contact with the cathode blocks. The upper layer is the electrolyte, into which are immersed the anodes.

ESTER calculates the height of the metal-electrolyte interface above the cathode surface. The interface adjustment is based on the principle of maintaining hydrostatic equilibrium across the interface. A reference cell is chosen (the first unblocked cell), and height adjustments are calculated for all other cells based on the pressure difference between the reference cells above and below the interface. Once the adjustments have been applied, the whole interface is moved up or down by a uniform amount in order to preserve the open volume under it.

This quantity is used to recompute the vertical locations of the finite-volume grid, which thereby 'floats' as the calculation proceeds so as to follow the computed interfacial undulations. Thus, there is no question of a finite-volume cell containing a mixture of metal and electrolyte: each cell contains either metal or electrolyte.

This floating grid ensures that the abrupt changes of Lorentz force encountered at the metal-electrolyte interface is accommodated without difficulty. The interface height enters the calculation of the electrical potential, via the finite-difference grid distortions resulting from the floating grid. Hence, where the gap between the interface and the anode face is at a minimum the largest currents will be computed, for the equations will see this location as the path of least electrical resistance.

The Lorentz forces driving the flow cause pressure differences across the interface, which then deforms. The enormous difference in conductivity between metal and electrolyte means that even small changes in interface height can significantly alter the resistance paths, and hence current distributions. This then feeds back to the Lorentz forces and the height distribution.

In ESTER, the interface is always maintained at the high faces of the top slab in the metal, slab IZ = IZ1. The grid is then stretched to follow the motion of the interface. Every slab below and above the interface is adjusted proportionally to avoid stretching or squeezing individual slabs too much.

3.1 Constant ACD

In steady-state cell operation, the anode bottom takes on the shape of the bath-metal interface, because the anode consumption is proportional to anode current density. Should the anode-cathode distance (ACD) be smaller than average under some anode, the current in the anode will be higher and the anode will consume faster until ACD is equal everywhere. This adjustment process lasts a few days, but eventually the cell assumes constant ACD. In ESTER, the bottom of the anode automatically adjusts to the metal pad shape to keep ACD constant if the “ACD Constant” toggle is activated. Otherwise, the anode surface stays flat, and this option is used in wave calculations.

4. Boundary Conditions

4.1 Electrical Boundary Conditions

Electrical boundary conditions are:

- Voltage and/or current specified on all external surfaces of the domain;
- At internal interfaces between different materials, normal component of current density and tangential component of electric field are conserved.

In the full Model 1, the current is specified in the collector bars, and the current entering the anode beam via anode risers is also specified. One reference voltage is fixed at the end of anode beam as shown in Figure 1. In Model 2, the vertical current density distribution on the top of the cathode

blocks is specified in an input file. In Model 3, the bottom is like in Model 2 and the anode beam is like in Model 1.

Internal boundaries are interfaces between materials. The most important one is the metal-bath interface. The same boundary conditions also apply to anode-bath, anode stub-anode carbon, and metal pad to top of cathode block. The numerical difficulty in all these is large difference in electrical conductivity between the materials in contact.

For interfaces between the materials, Equations (1)-(3), from electromagnetic theory, show the normal current density and tangential electric field conservation, Equation (1) in vector form, Equations (2) and (3) in scalar form.

$$\begin{aligned}(\mathbf{J_1}-\mathbf{J_2})\cdot\mathbf{n}&=\mathbf{0}\\(\mathbf{E_1}-\mathbf{E_2})\times\mathbf{n}&=\mathbf{0}\end{aligned} \tag{1}$$

$$J_{n1}=J_{n2}\text{ or }\sigma_1\left(\frac{\partial\phi}{\partial n}\right)_1=\sigma_2\left(\frac{\partial\phi}{\partial n}\right)_2 \tag{2}$$

$$E_{t1}=E_{t2}\text{ or}\left(\frac{\partial\phi}{\partial t}\right)_1=\left(\frac{\partial\phi}{\partial t}\right)_2 \tag{3}$$

where:

J	Current density vector
E	Electric field vector
n	Unit vector, normal to the surface
n	Normal component
t	Tangential component
1	Interface approached from material 1
2	Interface approached from material 2
ϕ	Electrical potential.

Figure 10 shows two current density vectors breaking at an interface, say bath (above) and metal (below). From Equations (2) and (3), we can determine the relationship between the angles.

From Equation (2),

$$J_1\cos\theta_1=J_2\cos\theta_2 \tag{3}$$

For the conservation of the tangential component of the electric field, we use Equation (4) first:

$$\mathbf{J}=-\sigma\nabla\phi=\sigma\mathbf{E} \tag{4}$$

$$E_{t1}=E_1\sin\theta_1=E_{t2}=E_2\sin\theta_2 \tag{5}$$

or

$$\frac{J_1\sin\theta_1}{\sigma_1}=\frac{J_2\sin\theta_2}{\sigma_2} \tag{6}$$

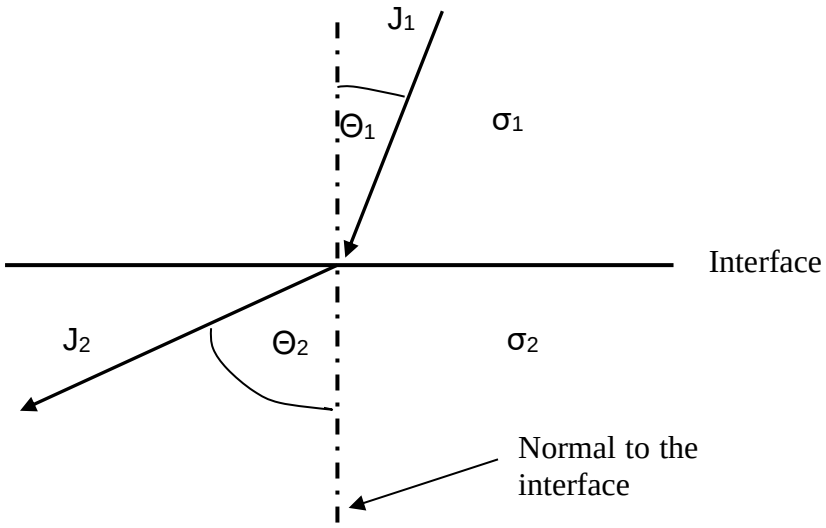

Figure 10. Geometry for current density vectors at a horizontal interface between two materials with different electrical conductivities, σ_1 and σ_2.

We can eliminate current densities if we divide Equation (6) by Equation (3), and we get the rule of current density "refraction" at the interface:

$$\frac{tg\theta_1}{tg\theta_2} = \frac{\sigma_1}{\sigma_2} \tag{7}$$

ESTER uses harmonic average of electrical conductivities at the metal bath interface defined with Equation (8):

$$\sigma_i = \frac{2\sigma_1\sigma_2}{\sigma_1 + \sigma_2} \tag{8}$$

It can be shown that Equation (8) is obtained if we apply boundary condition Equations (3-7) to the numerical analysis of the finite volume equations in the two slabs, one above and one below the interface. Therefore, ESTER correctly calculates the current refraction at the interface.

An interesting physical result comes out of Equation (7). Table 1 shows the relationship between θ_1 and θ_2 for bath-metal interface and metal-cathode carbon interface. This shows that the current density vector is practically always perpendicular to the metal bath interface from the bath side (in the material with low conductivity) and goes perpendicularly down from the metal-cathode carbon interface to the cathode carbon (in the material with low conductivity). This confirms that the specification of vertical current density at the top of cathode blocs in ESTER Model 2 and Model 3 is based on fundamental physics. In the metal, the direction of the current is inclined with respect to the two interfaces.

Table 1. Relationship between θ1 and θ2 for cell internal interfaces.

Bath-metal interface (material 2 has high conductivity)		**Metal-cathode carbon (material 1 has high conductivity)**	
θ_2	Θ_1**, bath to metal**	θ_1	θ_2**, metal to cathode carbon**
2	0.0001	2	0.01
5	0.0003	5	0.03
10	0.0005	10	0.06
22.5	0.001	22.5	0.13
45	0.003	45	0.31
60	0.005	60	0.54
85	0.04	85	3.5
89	0.18	89	17
89.9	1.8	89.9	72

The same calculation can be made for other interfaces: anode-bath, anode stub to carbon and cathode carbon to collector bars.

4.2 Magnetic Field

For all three ESTER models, magnetic field has to be specified. There are two options: Built in ESTER is a polynomial representation of second order of B_x, B_y and B_z. The user just specifies the polynomial coefficients for each particular case. The second option is that the magnetic field is specified in an input file.

4.3 Pressure

Pressure is continuous across the metal-bath interface: $p_{bath} = p_{metal}$. The movement of the interface is calculated from this condition as already explained in Section 3.

5. ESTER/PHOENICS Equations

PHOENICS solves a general conservation equation, which for a single-phase flow may be written as:

$$\frac{\partial(\rho\phi)}{\partial t} + \nabla(\rho u\phi - \Gamma_\phi \nabla\phi) = S_\phi \tag{9}$$

where:
ϕ The conserved quantity in question (e.g., momentum, energy, mass, etc.)
ρ Density
u Velocity vector
Γ_ϕ Diffusive exchange coefficient
S_ϕ Source term.

The source term and exchange coefficient vary from equation to equation, and also from case to case. Examples of source term are pressure gradient and gravity force for the momentum

equations, or kinetic heating for the enthalpy equation. The mass continuity equation can also be written in the above form by setting Γ_ϕ =1and S_ϕ=0.

In ESTER, the Lorenz force Equation (10) is a source in Equation (9).

$$\mathbf{F} = \mathbf{J} \times \mathbf{B} \tag{10}$$

where:

F Lorenz force vector
J Current density
B Magnetic induction vector
x Vector cross-product.

The commonly appearing sources, such as those mentioned above, are pre-programmed into the PHOENICS solver, EARTH. Provision is then made to enable users to add in any further sources required.

Conservation equations in traditional form are given in [2] and will not be repeated here.

6. Numerical Solution and Staggered Grid

The partial differential equation above is integrated over 'control volumes' (cells) to form the finite volume equation that is actually solved. For this purpose, the solution domain is subdivided into a number of control volumes on a mono-block mesh using a conventional staggered-grid approach. All field variables except velocities are stored at the grid nodes, while the velocities themselves are stored at staggered cell-face locations which lie between the nodes. In ESTER, the potential, being a scalar, is stored at the cell centres. The currents, being components of a vector, are stored at the cell faces. In the calculation of the Lorentz force, for each current component four currents must be averaged to the relevant cell face, taking into account non uniformities of the grid. To avoid the interpolation complications associated with the current components, the B field components are deemed to be stored at the cell centres, even though they too are strictly vectors.

The linkage between velocity, pressure and continuity is resolved by a variant of the SIMPLE algorithm**.**

The convergence requirement is that for each set of finite-volume equations the sum of the absolute residual sources over the whole solution domain is less than one percent of references quantities based on the total inflow of the variable in question. An additional requirement is that the values of monitored dependent variables at a selected location do not change by more than 0.1 percent between successive iteration cycles. It is also possible to monitor the absolute values of the largest corrections to each variable anywhere in the domain. It is also possible to specify the number of SWEEPs (global iterations) to stop the iterations. The sufficient number of sweeps is based on experience.

7. Turbulence Models

PHOENICS has the choice of many turbulence models. In ESTER, there is constant turbulent viscosity model. The constant viscosity model multiplies the laminar viscosity in the liquids with a constant to obtain the turbulent viscosity. The right value is chosen by model validation with the measured metal velocities. On the other hand, k-ε and k-ω model solve two partial differential equations to obtain turbulent viscosity. With the option of algebraic averaging of velocities, the best overall fit to the measured velocities was obtained with constant turbulent viscosity.

8. Model Validation

8.1 Bath-Metal Interface Waves and Metal Velocities

ESTER validation was made in [1] by measurements of metal-bath interface waves, using individual anode current measurements. A video record of those waves, shown at the TMS 1989 Annual Meeting, shows that the measured rotating wave compares well with ESTER calculations of the rotating wave shown in [1]. Other ESTER validations compare the measured metal velocities with ESTER calculations [4, 5]. Figure 11 shows the comparison of metal velocities between ESTER calculations and measurements in two cells [5]. Except for a few locations, very good agreement was observed between the two patterns, both in terms of magnitude and direction. This confirms once again the validity of ESTER metal velocity calculations.

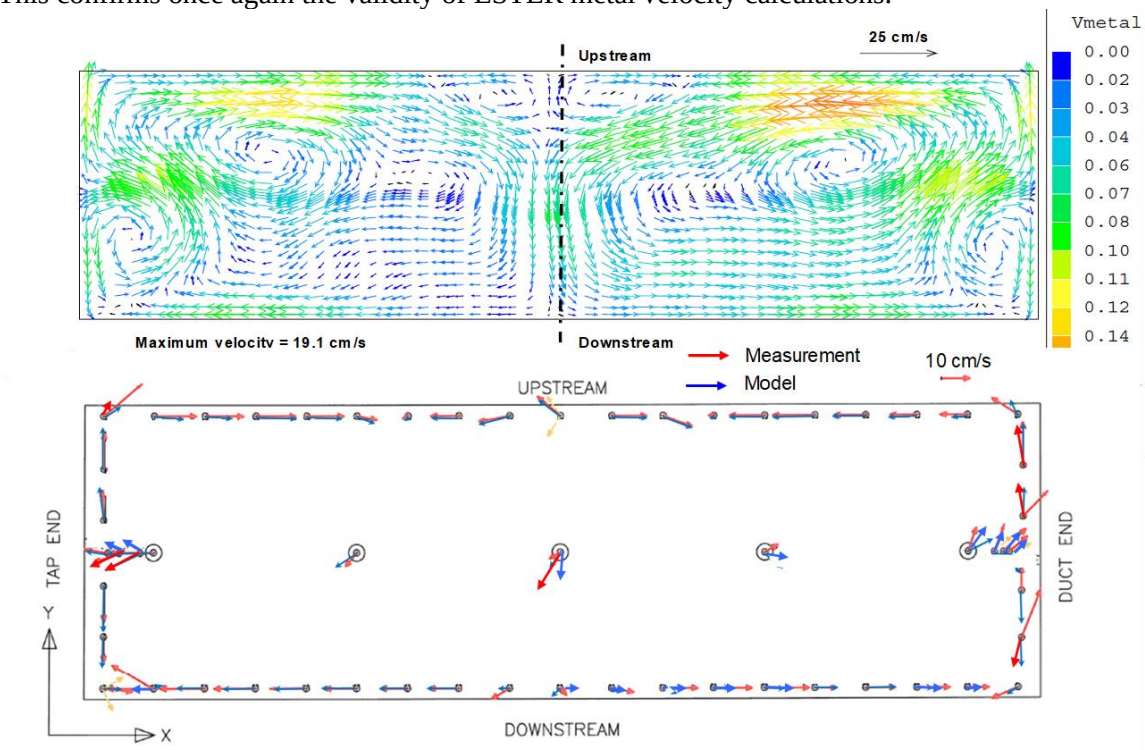

Figure 11. ESTER metal circulation patterns with calibrated velocity magnitudes in DX+ cells at 420 kA. Top – ESTER simulation with constant viscosity; bottom– measured metal velocities in 2 cells [5].

The k-ε model gave much higher viscosity in certain areas of the metal where velocities change rapidly in space such as in the upstream corners of the cell; this seems to slow down the metal too much on the average. In general, the lower the viscosity the more the force pattern imprints on the flow and the transitions from one pool to another become sharper. On the other hand, the velocity magnitudes increase with decreasing viscosity. The viscosity retained in our simulations gave the best compromise for fitting velocity pattern and magnitude to the measured velocities.

8.2 Bath-Metal Interface Heave

The validation of bath-metal interface heave is reported in [6]. Measurements in Albras cells reported previously were used. Figure 12 shows the comparison of the metal shape along the longitudinal axis of the cell. We can see very good agreement between ESTER and the measurements.

Another way to validate the model results is to compare different software packages. Interface profile on the longitudinal axis located at the center of the cell, calculated by three different packages used in the comparative study [6] is shown in Figure 13. In this comparison, the benchmark case was used. The interface is inclined in the positive direction because of asymmetry in the transverse component of the magnetic field, B_y. The agreement among the three software packages is excellent.

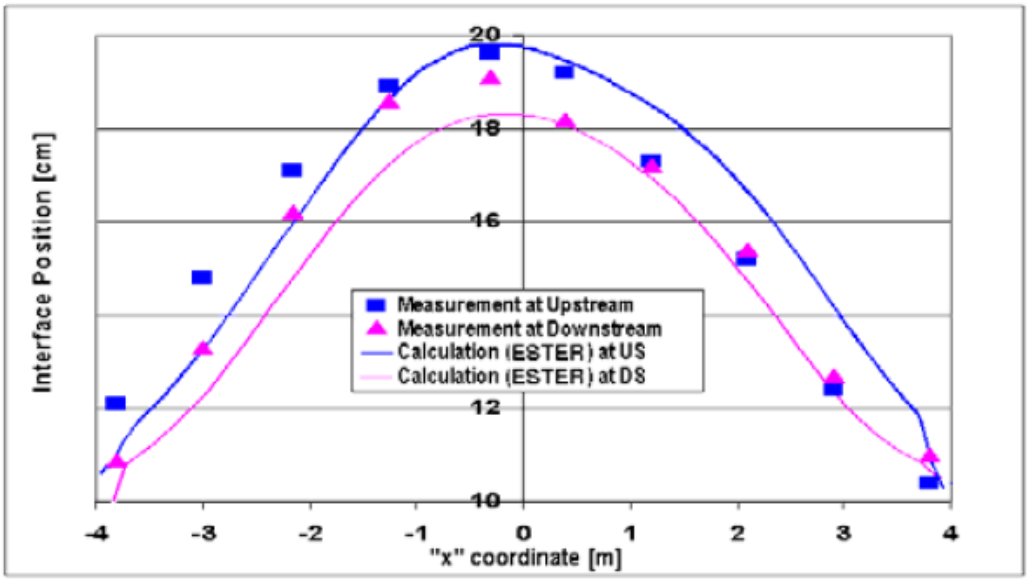

Figure 12. Metal-bath interface shape, calculated by ESTER versus measured by Albras.

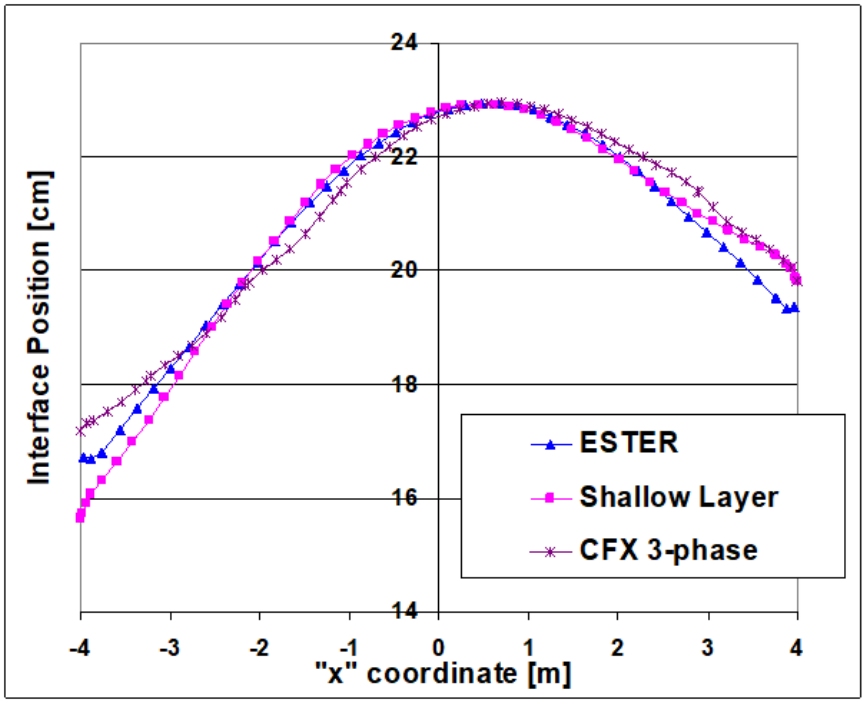

Figure 13. Comparison of calculated interface profiles for the benchmark case, calculated with different software packages [6].

9. Conclusions

The upgraded ESTER/PHOENICS is a user-friendly software package for the calculation of 3D MHD of aluminium electrolysis cells. It is designed so that no programming skill is required to run it. It calculates steady-state circulation of the bath and metal, metal heave and 3D waves of metal-bath interface. The calculation of metal velocities, interface heave and waves has been validated with measurements in various cell designs. During more than 30 years, ESTER has proven to be a valuable tool in cell MHD design.

Acknowledgement

The authors would like to thank Emirates Global Aluminium and Hindalco for the support of this ESTER upgrade.

10. References

1. Vinko Potocnik, Modelling of metal-bath Interface waves in Hall-Héroult cells using ESTER/PHOENICS, *Light Metals*1989, 227-235.
2. Amit Jha, Magnetic compensation loop design using transient ESTER/PHOENICS MHD simulations, *Proceedings of the 40th International ICSOBA Conference*, Athens, Greece, 10-14 October 2022, *Travaux* 51, Paper AL18.
3. John C. Ludwig and A. Adam, PHOENICS-ESTER User Guide, CHAM/TR315, 21 July 2021.
4. Vinko Potocnik, Frédéric L. Laroche, Comparison of measured and calculated metal pad velocities for different prebake cell designs, *Light Metals* 2001, 419-425.
5. Abdalla Zarouni, Lalit Mishra, Marwan Bastaki, Amal Al Jasmi, Alexander Arkhipov, Vinko Potocnik, Mathematical model validation of aluminium electrolysis cells at DUBAL, *Light Metals* 2013, 597-602.
6. Dagoberto S. Severo, Vanderlei Gusberti, André F. Schneider, Elton C. V. Pinto, Vinko Potocnik, Comparison of various methods for modeling the metal-bath interface, *Light Metals* 2008, 413-418.